Density variation effects in $\alpha + {}^{208}$Pb and ^{16}O + ^{208}Pb fusion reactions

Kaixuan Cheng,[1,2,*] Chang Xu,[2,†] Chunwang Ma,[1,‡] Jie Pu,[1] and Yuting Wang[1]
[1]*Institute of Particle and Nuclear Physics, Henan Normal University, Xinxiang 453007, China*
[2]*Department of Physics, Nanjing University, Nanjing 210008, China*

(Received 20 October 2020; accepted 15 January 2021; published 27 January 2021)

We propose a hybrid approach between the sudden model and the adiabatic model to explain the fusion hindrance in heavy-ion fusion reactions at deep subbarrier energies. Due to the strong Pauli blocking effects at the density overlap region, the α particle approaching the target ^{208}Pb becomes enlarged and its density distribution gets changed. By introducing energy dependence into this density variation effect, the potentials at different colliding energies are diverse. With the decrease of colliding energies, the significantly enhanced density variation effects make the nuclear potential more attractive and result in a deeper pocket in the inner part. A reasonable description of the experimental fusion cross sections is achieved for the $\alpha + {}^{208}$Pb reaction. On account of highlighting the influence of density variation effects on the fusion process at deep subbarrier energies, we further investigate the density variation effects in the ^{16}O + ^{208}Pb fusion reaction based on the α-cluster structures in ^{16}O nuclei. The fusion hindrance at deep subbarrier energies is described well by considering the density variation effects. In addition, an astrophysical S factor between the sudden model and adiabatic model is predicted at the energies below the experimental data.

DOI: 10.1103/PhysRevC.103.014613

I. INTRODUCTION

The fusion hindrance phenomenon observed recently at deep subbarrier energies in heavy-ion fusion reactions presents a challenge to current fusion theory [1]. The source of this steep fall-off feature in experimental fusion cross sections is not only helpful in understanding the properties of heavy nuclei but also interesting in clarifying the reaction mechanism, especially the nuclear reactions that occur in stars [2]. At the colliding energies close to the Coulomb barrier, it is assumed that a compound nucleus is formed automatically once the projectile penetrates the Coulomb barrier [3], and the coupled-channels (CC) approach has been successful in describing the fusion process [4–7]. With the colliding energies decreasing far below the Coulomb barrier, the projectile nucleus is still in the classically forbidden region when two colliding nuclei touch each other and the experimental fusion cross sections are overestimated by the results of the CC model [1,8–11]. This phenomenon indicates that the density overlap between projectile and target at extremely low colliding energies hinders the synthesis of the compound nucleus and has generated renewed interest in heavy-ion fusion reactions [12–26].

At deep subbarrier energies, dealing with the relationship between fusion and density variation of two reactants after touching is interesting. Thus, two different models have been proposed so far in order to describe the transformation from projectile and target to compound nucleus, namely, the sudden model [14–16] and the adiabatic model [17,18]. In the sudden model [14], Mişicu and Esbensen assumed that the densities of the two colliding nuclei are frozen and introduced a strong repulsive core to the nuclear potential to simulate the saturation properties of nuclear matter. On the other hand, Ichikawa *et al.* proposed an adiabatic approach by hypothesizing that fusion occurs so slowly that the density distribution has enough time to change [17] and constructed an adiabatic one-body potential to describe the neck formation between two colliding nuclei in the overlapping region [17,18]. Although the origins of the two models are considerably different from each other, the fusion hindrance at deep subbarrier energies can be described equally well by these two models [14,17]. Recently, inspired by the studies of α-cluster decay in radioactive nuclei [27–29], a preliminary work about the density overlap in α-induced and $n\alpha$-nuclei-induced fusion reactions also provided a good description of the fusion cross sections for $\alpha + {}^{208}$Pb, ^{16}O + ^{208}Pb, etc. reactions based on the sudden approximation [30,31].

In the literature [12], in order to remove the sudden approximation, namely, avoid the density of the compound system exceeding the central density of nucleus ^{32}S in ^{16}O + ^{16}O fusion reaction, Reichstein and Malik employed a special adiabatic approach to calculate the ^{16}O-^{16}O potential by introducing a distance dependence into the density parameters, picturing a transformation from the density distributions of reactants to that of a compound nucleus [12]. Interestingly, in studies of α-cluster decay in radioactive nuclei [27,32], Röpke *et al.* have revealed that due to the strong Pauli blocking effects, the α particle is very sensitive to the surrounding matter [27,32]. When approaching the nucleus ^{208}Pb, the α particle

*chengkaixuan@htu.edu.cn
†cxu@nju.edu.cn
‡machw@htu.edu.cn

dissolves at the density overlap region and its four nucleons gets mixed up with surrounding matter, which means that the α-particle size increases and the density distribution changes with the decrease of the distance between the center of mass of α particle and ^{208}Pb nucleus [27]. By considering this effect, a significant improvement is achieved in calculating the half-life of α decays [33,34].

As a reverse quantum tunneling process with decay, the projectile α particles in fusion reactions should also suffer the density variation at the density overlap region. In addition, in literature [22,23,35–37], the energy dependence of the nucleus-nucleus potential has been demonstrated to have an important role on fusion. So, in this paper, we not only introduce the density variation effect (DVE) of α particle in $\alpha + {}^{208}$Pb fusion reaction but also consider the energy dependence of this effect. Then, according to the α-cluster structures in the ^{16}O nucleus, we analyze the contributions of DVE to the potential for $^{16}\mathrm{O} + {}^{208}$Pb fusion system and study its influence on fusion hindrance at deep subbarrier energies.

The rest of paper is organized as follows. In Sec. II, we first describe the potential formulation and how to introduce the density variation effects. Then the theoretical framework of coupled-channels model is presented simply. In Sec. III, the contributions of density variation in $\alpha + {}^{208}$Pb and $^{16}\mathrm{O} + {}^{208}$Pb fusion reactions to potentials and fusion cross sections are discussed. The summary is displayed in Sec. IV.

II. THEORETICAL FRAMEWORK

A. Heavy-ion potential

First, we give the explicit form of the potential between projectile and target used in our calculations. In the literature [30,31], it is concluded that in addition to the attractive nuclear interaction and the repulsive Coulomb interaction, there is a non-negligible Pauli repulsive interaction between two colliding nuclei. When the projectile and target nuclei start touching each other, the Pauli blocking effects become increasingly important owing to the density overlap. To this end, a Pauli blocking potential, V_P, as the consequence of antisymmetrization, is introduced to replace the exchange term in the standard Michigan-3-Yukawa (M3Y) potential as follows [30,31]:

$$V_N(\mathbf{R}) = \int d\mathbf{r_1} d\mathbf{r_2} \rho_p(\mathbf{r_1}) \rho_t(\mathbf{r_2}) g(|\mathbf{s}|) + V_P(\mathbf{R}), \quad (1)$$

with

$$g(|\mathbf{s}|) = c_1 \frac{\exp(-4s)}{4s} - c_2 \frac{\exp(-2.5s)}{2.5s}. \quad (2)$$

In Eq. (1), the symbol $\mathbf{R}$ denotes the distance between the center of mass of two colliding nuclei and the quantity $|\mathbf{s}|(\mathbf{s} = \mathbf{R} - \mathbf{r_1} + \mathbf{r_2})$ is the distance between a nucleon in the target and a nucleon in the projectile. The parameters c_1 and c_2 in Eq. (2) are the strength of the Yukawa interactions and their fitted values are $c_1 = 11423$ MeV fm and $c_2 = 3551$ MeV fm, respectively. For convenience, we label this nuclear interaction as "M3Y + Pauli" potential.

The density distribution of projectiles ρ_p employed in Eq. (1) is a standard Gaussian form for α particle [38–40] or a modified Gaussian form for ^{16}O nucleus [41,42],

$$\rho_p^{\alpha}(r) = \rho_0^{\alpha} \exp(-\beta_0 r^2), \quad (3)$$

$$\rho_p^{O}(r) = \rho_0^{O}(1 + \omega r^2) \exp(-\gamma r^2), \quad (4)$$

where the parameters β_0, ω, and γ are obtained by fitting the corresponding root mean square (rms) radii and their values used in calculations are 0.7024, 0.6457, and 0.3228 fm^{-2}, respectively [38,42]. ρ_0 is determined by integrating the density distribution equivalent to the corresponding mass number.

The density distribution of target ρ_t adopted in Eq. (1) is given by the standard Fermi form [43]

$$\rho_t(r) = \frac{\rho_{0t}}{1 + \exp(\frac{r-c}{a})}, \quad (5)$$

in which c and a are half-density radius and diffuseness parameters and ρ_{0t} is determined by the normalization condition. The proton and neutron density parameters used in calculations for ^{208}Pb nuclei are $c_p = 6.68$, $a_p = 0.447$, $c_n = 6.7$, and $a_n = 0.55$ fm [27].

The Pauli blocking potential V_P in Eq. (1) for the α particle is obtained by solving the in-medium four-nucleon wave equation with a variational approach, and a good fit formula is given by [27]

$$V_P^{\alpha}(\rho_t) = 4515.9\rho_t - 100935\rho_t^2 + 1202538\rho_t^3. \quad (6)$$

As a reverse quantum tunneling process with fusion, this Pauli blocking potential has been successfully applied to the radioactive α-cluster decay in heavy nuclei and superheavy nuclei [27–29]. For the ^{16}O nucleus, the Pauli blocking potential is constructed by using a single folding procedure [31],

$$V_P^{O}(\mathbf{R}) = \int \rho_c(\mathbf{r}') V_p^{\alpha}(\mathbf{R} + \mathbf{r}') d\mathbf{r}', \quad (7)$$

where ρ_c is the α-cluster distribution function in $n\alpha$ nuclei and satisfies the condition [41]

$$\rho_p^{O}(\mathbf{r}) = \int \rho_c(\mathbf{r}') \rho_p^{\alpha}(|\mathbf{r} - \mathbf{r}'|) d\mathbf{r}'. \quad (8)$$

By using the Fourier transform techniques [38], the α-cluster distribution function $\rho_c(r)$ can be given by [42]

$$\rho_c(r) = \rho_{0c}(1 + \mu r^2) \exp(-\xi r^2), \quad (9)$$

with

$$\eta = \beta_0 - \gamma, \quad \xi = \gamma\beta_0/\eta, \quad \mu = \frac{2\omega\beta_0^2}{\eta(2\eta - 3\omega)}, \quad (10)$$

where ρ_{0c} is obtained by integrating Eq. (8) equivalent to the mass number of projectiles.

The Coulomb potential employed in calculations is the double-folding integral of the proton-proton Coulomb interaction

$$V_C(\mathbf{R}) = \int d\mathbf{r_1} d\mathbf{r_2} \frac{e^2}{|\mathbf{s}|} \rho_{pp}(\mathbf{r_1}) \rho_{tp}(\mathbf{r_2}), \quad (11)$$

where ρ_{pp} and ρ_{tp} denote the proton density distributions of the projectile and target nucleus, respectively.

B. Density variation effect

In the literature [32], Röpke concluded that the α particles are sensitive to Pauli blocking from the surrounding matter (or target nuclei). At the critical distance, this α particle approaching the target dissolves and its four nucleons get mixed up with the surrounding Fermi gas. Here, this dissolving effect of the α particle is introduced into the fusion reactions. So the width parameter β of the α particle is employed as a function of the density of target ρ_t (or characterized by the distance between the center of mass of two colliding nuclei R) by

$$\beta(\rho_t, E) = \beta(R, E) = \frac{\beta_0}{1 + \exp(-\frac{R-R_c}{a_c})}, \tag{12}$$

and now the density distribution of α particle is obtained by

$$\rho_p^{\alpha}(r, R, E) = \rho_0^{\alpha} \exp(-\beta r^2). \tag{13}$$

In Eq. (12), β_0 is the width parameter of α particle at infinity (or free α particle) and R_c is dissolving radius given by $R_c = 1.2(A_p + A_t)^{1/3}$ fm.

The parameter a_c in Eq. (12) is the dissolving diffuseness parameter depending on the colliding energies E and can be obtained by $a_c = a_0 V_b/E$. This indicates that when the colliding energy is relatively low, the fusion reaction slows down so that the projectile has enough time to change its density distribution. In contrast, a fast fusion occurs at the high colliding energies and corresponds to a sudden picture. For simplicity, the strength a_0 is assumed to be unity and the values of Coulomb barrier V_b are 20.6 MeV for $\alpha + {}^{208}$Pb fusion system [44] and 75.65 MeV for ^{16}O + ^{208}Pb fusion system [16].

For nucleus ^{16}O, Eq. (9) shows its α-cluster distribution function under the free condition. Here, we approximately assume this distribution function is fixed and still valid as projectile ^{16}O approaches the target. Then the density of ^{16}O nucleus with DVE can be obtained from Eq. (8) by inserting Eq. (13).

Note that when the projectile α particle or ^{16}O nucleus is approaching the target, the density of nucleus ^{208}Pb should also be transformed into that of compound nucleus. However, due to extreme asymmetry of mass between the projectile and target in the fusion systems studied here, the DVE of the target ^{208}Pb is very weak and negligible. In addition, the Pauli blocking potential obtained from Eq. (6) is only dependent on the density of target and is consistent with or without DVE.

C. Coupled-channels model

We apply the CCFULL code to calculate the fusion cross sections [45,46]. In the calculations, the incoming wave boundary condition (IWBC) is imposed and the absorption radius is taken to be at the minimum of the potential inside the Coulomb barrier [45,46]. With the IWBC, the coupled-channels equations can be given by [45]

$$\left[-\frac{\hbar^2}{2\mu}\frac{d^2}{dR^2} + \frac{J(J+1)\hbar^2}{2\mu R^2} + V(R) + \epsilon_n - E\right]u_n(R) + \sum_m V_{nm}(R)u_m(R) = 0, \tag{14}$$

where E is the incident energy in the center-of-mass frame, ϵ_n is the excitation energy of the nth channel, and u_n is the radial wave function of the nth channel. The total potential $V(R)$ between two colliding nuclei consists of both Coulomb and nuclear interactions, i.e., $V(R) = V_N(R) + V_C(R)$ and is associated with the incident energies by considering the DVE.

The symbol $V_{nm}(R)$ in Eq. (14) denotes the matrix of the coupling Hamiltonian which includes both the Coulomb and nuclear components. The Coulomb coupling matrix elements V_{nm}^C are calculated by the linear coupling approximation [4,45,46]. The nuclear coupling Hamiltonian is generated by introducing a dynamical operator $\hat{O}_\lambda$ in the calculations and given by $\widetilde{V}_N(R, \hat{O}_\lambda) = V_N(R - \hat{O}_\lambda)$ [45,46]. For the vibrational coupling, the operator $\hat{O}_\lambda$ is given by $\hat{O}_\lambda = (\beta^*/\sqrt{4\pi})R_i(\alpha_{\lambda 0}^\dagger + \alpha_{\lambda 0})$ [4,45,46], where $\alpha_{\lambda 0}^\dagger$ and $\alpha_{\lambda 0}$ are the creation and annihilation operators of the phonons, respectively, the eigenvalues λ and eigenvectors $|\alpha\rangle$ of the operator $\hat{O}$ satisfy $\hat{O}_\lambda|\alpha\rangle = \lambda_\alpha|\alpha\rangle$, R_i is the radius of the projectile or target, and β^* denotes the corresponding deformation parameter. The nuclear coupling matrix elements are then evaluated by [4,45,46]

$$\begin{aligned} V_{nm}^N &= \langle n|\widetilde{V}_N(R, \hat{O}_\lambda)|m\rangle - V_N(R)\delta_{n,m} \\ &= \sum_\alpha \langle n|\alpha\rangle\langle\alpha|m\rangle \widetilde{V}_N(R, \lambda_\alpha) - V_N(R)\delta_{n,m}. \end{aligned} \tag{15}$$

The nuclear coupling potential $\widetilde{V}_N(R, \lambda_\alpha) = V_N(R - \lambda_\alpha)$ is taken up to the second order of λ_α [4,45,46]

$$\widetilde{V}_N(R, \lambda_\alpha) = V_N(R) - \frac{dV_N(R)}{dR}\lambda_\alpha + \frac{1}{2}\frac{d^2V_N(R)}{dR^2}\lambda_\alpha^2, \tag{16}$$

where the first term $V_N(R)$ is the nuclear potential in the absence of the coupling and the second and third terms are the nuclear coupling form factor, which are closely associated with the nuclear potential.

By solving the CC equations, the penetrability P_J can be obtained and the total fusion cross section $\sigma_{\rm fus}$ is then given by summing the partial fusion cross section [45]

$$\sigma_{\rm fus}(E) = \frac{\pi}{k^2}\sum_J (2J+1)P_J(E), \tag{17}$$

where $k = \sqrt{2\mu E/\hbar^2}$ is the wave number associated with the energy E. Here, it is noted that the fusion cross section with DVE is calculated from the potential at each colliding energy.

III. RESULTS AND DISCUSSION

A. α + ^{208}Pb

We first study the effect of density variation in the α + ^{208}Pb fusion reaction. In Fig. 1, it is shown that by considering DVE, the values of width parameter β and corresponding central density ρ_0 of α particle decrease significantly along with the decrease of distance between the centers of mass of two colliding nuclei. The energies of 23.5 MeV (dotted line) and 15.6 MeV (dashed line) correspond to the two extreme energy values in the current experimental data in Ref. [44], namely, the maximum colliding energy and minimum colliding energy, respectively. At energy of 15.6 MeV, the fusion reaction occurs relatively more slowly and the density of the

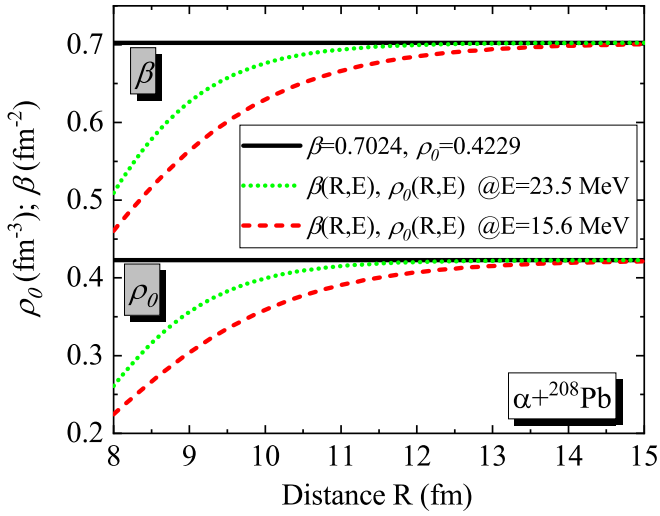

FIG. 1. The width parameter β and corresponding central density ρ_0 of α particle vs the distance between the center of mass of two nuclei at energies of 23.5 MeV (dotted line) and 15.6 MeV (dashed line) for $\alpha + {}^{208}$Pb fusion reaction. The solid lines denote the results without considering DVE.

α particle has enough time to redistribute. So there is a more obvious DVE at energy of 15.6 MeV than that at energy of 23.5 MeV.

The insert of Fig. 2 shows the potentials of M3Y + Pauli (solid line) and M3Y + Pauli + DVE at energies of 23.5 MeV (dotted line) and 15.6 MeV (dashed line). In the outer region, the role of DVE is negligible and the potentials have the same behavior. The geometry of the potential obviously varies in the inner region. By considering the DVE, a deeper

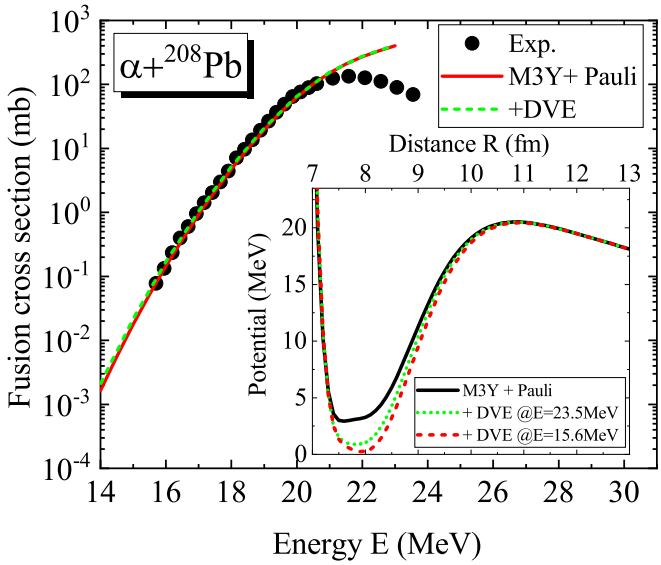

FIG. 2. The experimental cross sections for $\alpha + {}^{208}$Pb fusion reaction [44] compared with the results calculated by M3Y + Pauli potential (solid line) and M3Y + Pauli + DVE potential (dashed line). The insert shows the M3Y + Pauli potential (solid line) and M3Y + Pauli + DVE potentials at energies of 23.5 MeV (dotted line) and 15.6 MeV (dashed line).

pocket is generated as compared to the one obtained from the M3Y + Pauli potential. By ignoring the channel coupling for fusion reaction $\alpha + {}^{208}$Pb, we compare, in Fig. 2, the experimental fusion cross sections with the results calculated by M3Y + Pauli potential (solid line) and M3Y + Pauli + DVE potentials (dashed line). Good consistency is obtained between experimental data and the results calculated by the potentials with or without DVE at low-energy regions (approximately before 21 MeV, the decline in fusion data after 21 MeV results from the influence of neutron evaporation effects, i.e., the experimental data only contain the evaporation residue cross sections of the one-neutron evaporation channel and is short of the evaporation residue cross sections of two-neutron and three-neutron evaporation channels, which have been indicated to play a considerable role after the incident energy reaching about 21 MeV [44,47]). At the energies above 15.6 MeV, there is little difference between the potentials with or without DVE and the fusion cross sections obtained from these two potentials are almost the same. To further study the influence of DVE at deep subbarrier energies, next, we extended our calculations to fusion system ^{16}O + ^{208}Pb.

B. ^{16}O + ^{208}Pb

Approaching the target nuclei, there is considerable density variation of the projectile nuclei ^{16}O resulting from the DVE of the α-cluster components. For better understanding, the density distributions of ^{208}Pb nuclei, ^{16}O nuclei, and α cluster at Coulomb barrier energy 75.65 MeV are shown in Fig. 3 for distances R equivalent to 15, 11, 8, and 7 fm. Before density overlapping between projectile and target, the radii of ^{16}O and α clusters are almost the same as those in infinity, such as the rms radii of ^{16}O and α clusters being 2.64 and 1.46 fm at distance $R = 15$ fm. With the density overlapping, the α clusters dissolve and the projectile nuclei ^{16}O becomes looser due to the Pauli blocking effects. Therefore, at a strong density overlap region, such as at $R = 8$ fm, the rms radii of α clusters increase to 1.78 from 1.46 fm at $R = 15$ fm and the corresponding rms radius of the ^{16}O nucleus also increases to 2.83 from 2.64 fm. It can be seen that the density distributions of ^{16}O nucleus and α particle have changed considerably in Fig. 3.

In Fig. 4, we make a comparison between two potentials calculated by M3Y + Pauli with or without DVE. The nuclear, Coulomb, and Pauli blocking interactions are shown in Fig. 4(a) and the insert focuses on the difference between two nuclear interactions near $R = 9.6$ fm. Because we ignore the DVE of target nuclei and the changes of α cluster distribution function ρ_c in Eq. (7), the Pauli blocking interactions are the same with or without DVE. The difference of the Coulomb interactions is extremely small before $R = 7$ fm (about 1% at $R = 7$ fm). A sensitive dependence of density variation is embodied in the nuclear interaction; i.e., the increasing density distribution of ^{16}O nucleus causes a more attractive force in the M3Y + Pauli + DVE nuclear interaction. When further approaching, the repulsive Pauli blocking interaction rises steeply and dominates in nuclear interaction. A deeper pocket at the inner part of the total potential calculated with DVE is formed as shown in Fig. 4(b).

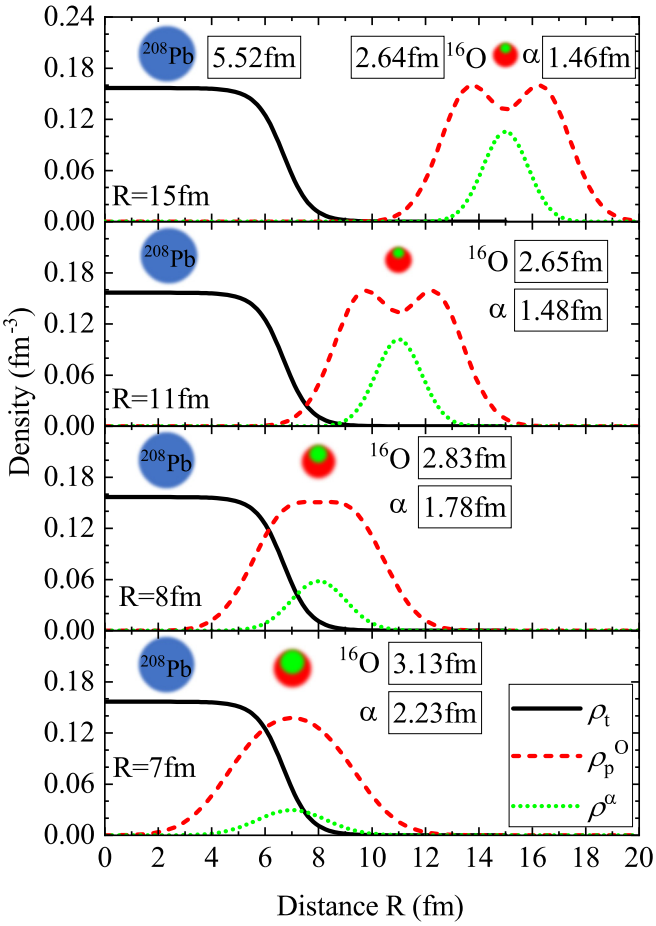

FIG. 3. The density variation of ^{16}O nuclei and α cluster approaching the target ^{208}Pb at colliding energy of 75.65 MeV. The solid, dashed, and dotted lines denote the density distributions of ^{208}Pb, ^{16}O, and α cluster, respectively. Note that the density of α cluster has been multiplied by 0.25. The numbers in box show the root-mean-square radii of corresponding nuclei at specified distance.

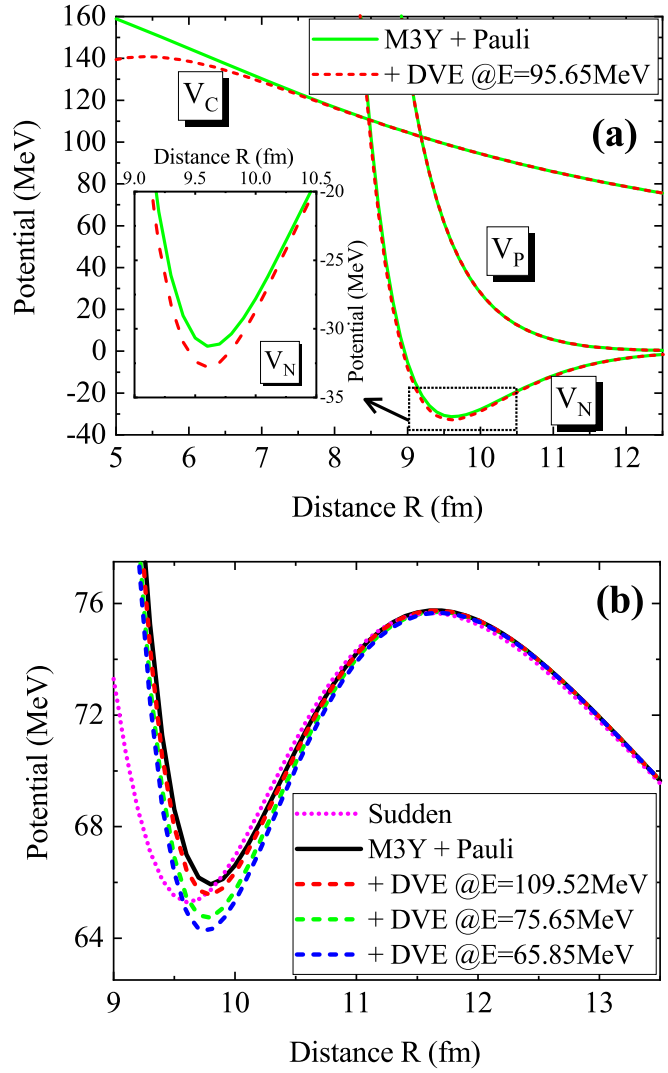

FIG. 4. (a) The comparison of the Coulomb potential V_C, Pauli blocking potential V_P, and nuclear potential V_N between M3Y + Pauli potential (solid line) and M3Y + Pauli + DVE potential (dashed line) at Coulomb barrier energy $E = V_b = 95.65$ MeV. (b) The comparison between M3Y + Pauli potential (solid line) and M3Y + Pauli + DVE potential (dashed line) at energy of 109.52, 95.65, and 65.85 MeV. The dotted line denotes M3Y + repulsive potential obtained from the sudden model [16].

The total potentials calculated by M3Y + Pauli with or without DVE are compared in Fig. 4(b). The energies of 109.52 and 65.85 MeV correspond to the maximum and minimum experimental colliding energies in Refs. [10,48]. The dotted line denotes the M3Y + repulsive potential extracted from the sudden model [16]. A similar shallow pocket is formed in the inner part of the potentials obtained from M3Y + repulsive interaction and M3Y + Pauli interactions with or without DVE. As a result of the sudden approach, the M3Y + Pauli potential (solid line) has a shallower pocket than that of potentials calculated by considering DVE (dashed lines). At high colliding energy $E = 109.52$ MeV, the fusion occur more quickly and the DVE has a weaker influence on the fusion. The M3Y + Pauli +DVE potential at energy $E = 109.52$ MeV is closer to the result of M3Y + Pauli. Along with the decrease of colliding energies, the influence of DVE is more obvious and a deeper pocket is generated, such as at energies $E =$ 95.65 and 65.85 MeV. This feature is consistent with the results of sudden model proposed by Mişicu and Esbensen by considering the incompressibility of nuclear matter. At above barrier energies, the density at the overlap region has no enough time to change, corresponding to a hard nuclear equation of state (EOS) in the sudden model [14–16], whereas the strong density variation at deep subbarrier energies could be described by a soft EOS and results in a deep pocket [14–16].

The fusion cross sections calculated by M3Y + Pauli potential with or without DVE are compared with the experimental data in Fig. 5. The experimental data is taken from the Refs. [10,48]. The parameters used in the calculations, namely, the multipolarity and the parity of a state λ^π, the excitation energy of a state E_{ex}, and deformation parameters β^* are the same as those used in Ref. [31]. In Fig. 5, the solid line is the no-coupling calculated fusion cross sections. The

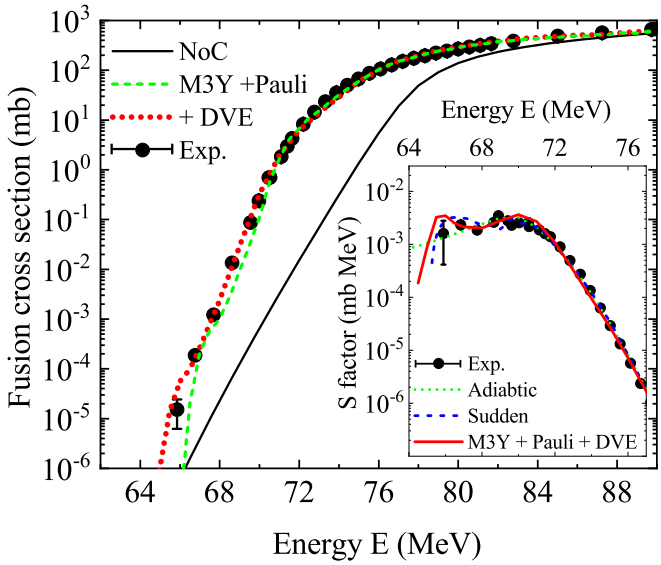

FIG. 5. The experimental fusion cross sections for ^{16}O + ^{208}Pb [10,48] fusion system compared with the CC calculations obtained by M3Y + Pauli potential (dashed line) and M3Y + Pauli + DVE potential (dotted line). The solid line denotes the no-coupling results of standard M3Y potential. The insert shows the comparison of S factors between experimental data and the results calculated by adiabatic model (dotted line), sudden model (dashed line), and M3Y + Pauli + DVE approach (solid line).

results calculated by M3Y + Pauli potential with or without DVE are denoted by dotted and dashed lines, respectively. The experimental data at deep subbarrier energies is underestimated by the M3Y + Pauli potential. A good agreement with the fusion data is obtained by the results with DVE. In addition, the astrophysical S factor representation is shown in the insert and it is seen that the S factor is well described by the results of the sudden model (dashed line), adiabatic model (dotted line), and M3Y + Pauli + DVE approach (solid line). Because of different assumptions, the sudden model and adiabatic model have diverse results at much deeper colliding energies. Interestingly, an intermediate result is presented by considering DVE.

IV. SUMMARY

In summary, we analyzed the influence of density variation effects on fusion reactions α + ^{208}Pb and ^{16}O + ^{208}Pb, especially on the fusion hindrance at deep subbarrier energies. When the densities of two colliding nuclei overlap, the α particle approaching the target ^{208}Pb becomes loose due to the strong Pauli blocking. A remarkable feature is that the radius of α particle increases with the decrease of the distance between the center of mass of two nuclei. By introducing the energy dependence, we simulated a transformation process from the sudden picture to the adiabatic picture. At above-barrier energies, the fusion takes place so quickly that the density of the α particle have no enough time to change, corresponding to a sudden approximation. Conversely, an obvious density variation effect works at deep subbarrier energies.

Based on the α cluster structures of ^{16}O nuclei, we introduces the density variation effect of α particle into ^{16}O + ^{208}Pb fusion reaction. Analogous to the α particle, the radius of projectile ^{16}O also becomes increased appreciably after the density overlapping. We found that the density variation effect results in a more attractive nuclear interaction as compared to the M3Y + Pauli potential and the significantly enhanced density variation effects make the potential pockets deeper with the decrease of colliding energies. By considering the density variation effects in ^{16}O + ^{208}Pb fusion reaction, the fusion cross sections and astrophysical S factor at deep subbarrier energies can be described well. In addition, a result of the S factor between the results of sudden model and adiabatic model is predicted below the experimental energies.

In this paper, we study the influences of density variation of α particles and $n\alpha$ nuclei ^{16}O. It will be interesting to extend the present calculation to more complicated fusion systems. Therefore, several further improvements are needed in the future. For instance, owing to the extreme asymmetry of mass, the influence of density variation of targets is neglected in our present calculations and it may be an obvious effect in symmetric systems, such as ^{64}Ni + ^{64}Ni fusion reaction. In addition, the influences of the density variation on the CC effects, such as the damping of coupling effect, which mainly plays a role at deep subbarrier energies [18,49,50], should also be taken into account next.

ACKNOWLEDGMENTS

The work is supported by the National Natural Science Foundation of China (Grants No. 11822503 and No. 11975091).

[1] C. L. Jiang, H. Esbensen, K. E. Rehm, B. B. Back, R. V. F. Janssens, J. A. Caggiano, P. Collon, J. Greene, A. M. Heinz, D. J. Henderson, I. Nishinaka, T. O. Pennington, and D. Seweryniak, Phys. Rev. Lett. **89**, 052701 (2002).
[2] C. L. Jiang, B. B. Back, H. Esbensen, R. V. F. Janssens, and K. E. Rehm, Phys. Rev. C **73**, 014613 (2006).
[3] T. Ichikawa, K. Hagino, and A. Iwamoto, Phys. Rev. C **75**, 064612 (2007).
[4] H. Esbensen and S. Landowne, Phys. Rev. C **35**, 2090 (1987).
[5] M. Dasgupta, A. Navin, Y. K. Aagrwal, C. V. K. Baba, H. C. Jain, M. L. Jhingan, and A. Roy, Nucl. Phys. A **539**, 351 (1992).
[6] K. Hagino, N. Takigawa, M. Dasgupta, D. J. Hinde, and J. R. Leigh, Phys. Rev. C **55**, 276 (1997).
[7] J. O. Newton, C. R. Morton, M. Dasgupta, J. R. Leigh, J. C. Mein, D. J. Hinde, H. Timmers, and K. Hagino, Phys. Rev. C **64**, 064608 (2001).
[8] C. L. Jiang, H. Esbensen, B. B. Back, R. V. F. Janssens, and K. E. Rehm, Phys. Rev. C **69**, 014604 (2004).

[9] C. L. Jiang, K. E. Rehm, R. V. F. Janssens, H. Esbensen, I. Ahmad, B. B. Back, P. Collon, C. N. Davids, J. P. Greene, D. J. Henderson, G. Mukherjee, R. C. Pardo, M. Paul, T. O. Pennington, D. Seweryniak, S. Sinha, and Z. Zhou, Phys. Rev. Lett. **93**, 012701 (2004).
[10] M. Dasgupta, D. J. Hinde, A. Diaz-Torres, B. Bouriquet, C. I. Low, G. J. Milburn, and J. O. Newton, Phys. Rev. Lett **99**, 192701 (2007).
[11] M. M. Hosamani, A. Vinayak, and N. M. Badiger, Nucl. Sci. Tech. **31**, 89 (2020).
[12] I. Reichstein and F. B. Malik, Phys. Lett. B **37**, 344 (1971).
[13] C. J. Lin, Phys. Rev. Lett. **91**, 229201 (2003).
[14] Ş. Mişicu and H. Esbensen, Phys. Rev. Lett **96**, 112701 (2006).
[15] Ş. Mişicu and H. Esbensen, Phys. Rev. C **75**, 034606 (2007).
[16] H. Esbensen and Ş. Mişicu, Phys. Rev. C **76**, 054609 (2007).
[17] T. Ichikawa, K. Hagino, and A. Iwamoto, Phys. Rev. Lett **103**, 202701 (2009).
[18] T. Ichikawa, Phys. Rev. C **92**, 064604 (2015).
[19] K. Hagino and Y. Watanabe, Phys. Rev. C **76**, 021601(R) (2007).
[20] A. Diaz-Torres, D. J. Hinde, M. Dasgupta, G. J. Milburn, and J. A. Tostevin, Phys. Rev. C **78**, 064604 (2008).
[21] A. S. Umar and V. E. Oberacker, Phys. Rev. C **74**, 021601(R) (2006).
[22] A. S. Umar, C. Simenel, and V. E. Oberacker, Phys. Rev. C **89**, 034611 (2014).
[23] V. Y. Denisov, Phys. Rev. C **89**, 044604 (2014).
[24] V. Y. Denisov, Phys. Rev. C **91**, 024603 (2015).
[25] E. Uegaki and Y. Abe, Prog. Theor. Phys. **90**, 615 (1993).
[26] V. V. Sargsyan, G. G. Adamian, N. V. Antonenko, W. Scheid, and H. Q. Zhang, Phys. Rev. C **84**, 064614 (2011).
[27] G. Röpke, P. Schuck, Y. Funaki, H. Horiuchi, Z. Ren, A. Tohsaki, C. Xu, T. Yamada, and B. Zhou, Phys. Rev. C **90**, 034304 (2014).
[28] C. Xu, Z. Ren, G. Röpke, P. Schuck, Y. Funaki, H. Horiuchi, A. Tohsaki, T. Yamada, and B. Zhou, Phys. Rev. C **93**, 011306(R) (2016).
[29] C. Xu, G. Röpke, P. Schuck, Z. Ren, Y. Funaki, H. Horiuchi, A. Tohsaki, T. Yamada, and B. Zhou, Phys. Rev. C **95**, 061306(R) (2017).
[30] K. Cheng and C. Xu, Phys. Rev. C **99**, 014607 (2019).
[31] K. Cheng and C. Xu, Phys. Rev. C **102**, 014619 (2020).
[32] G. Röpke, Nucl. Phys. A **867**, 66 (2011).
[33] D. Deng and Z. Ren, Phys. Rev. C **96**, 064306 (2017).
[34] D. Deng, Z. Ren, and N. Wang, Phys. Lett. B **795**, 554 (2019).
[35] K. Washiyama and D. Lacroix, Phys. Rev. C **78**, 024610 (2008).
[36] W. M. Seif, Nucl. Phys. A **767**, 92 (2006).
[37] Z. Q. Feng, G. M. Jin, and F. S. Zhang, Nucl. Phys. A **802**, 91 (2008).
[38] G. R. Satchler and W. G. Love, Phys. Rep. **55**, 183 (1979).
[39] C. Xu and Z. Ren, Phys. Rev. C **74**, 014304 (2006).
[40] J. Fan and C. Xu, Nucl. Phys. A **989**, 1 (2019).
[41] M. El-Azab Farid, Z. M. M. Mahmoud, and G. S. Hassan, Nucl. Phys. A **691**, 671 (2001).
[42] G. Kocak, M. Karakoc, I. Boztosun, and A. B. Balantekin, Phys. Rev. C **81**, 024615 (2010).
[43] A. Bohr and B. R. Mottelson, *Nuclear Structure* (World Scientific, Singapore, 1998), Vol. 1.
[44] A. R. Barnett and J. S. Lilley, Phys. Rev. C **9**, 2010 (1974).
[45] K. Hagino and N. Takigawa, Prog. Theor. Phys. **128**, 1061 (2012).
[46] K. Hagino, N. Rowley, and A. T. Kruppa, Comput. Phys. Commun. **123**, 143 (1999).
[47] V. I. Zagrebaev, Phys. Rev. C **67**, 061601(R) (2003).
[48] C. R. Morton, A. C. Berriman, M. Dasgupta, D. J. Hinde, J. O. Newton, K. Hagino, and I. J. Thompson, Phys. Rev. C **60**, 044608 (1999).
[49] T. Ichikawa and K. Matsuyanagi, Phys. Rev. C **88**, 011602(R) (2013).
[50] T. Ichikawa and K. Matsuyanagi, Phys. Rev. C **92**, 021602(R) (2015).